# Impact of specific fracture energy investigated in front of the crack tip of three-point bending specimen

J. Klon, J. Sobek, L. Malíková
*Brno University of Technology, Faculty of Civil Engineering, Institute of Structural Mechanics, Brno, Czech Republic*
*klon.j@fce.vutbr.cz, http://orcid.org/0000-0002-9551-2185*
*sobek.j@fce.vutbr.cz, http://orcid.org/0000-0003-4215-1029*
*malikova.l@fce.vutbr.cz, http://orcid.org/0000-0001-5868-5717*

S. Seitl
*Academy of Sciences of the Czech Republic, v. v. i., Institute of Physics of Materials, Brno, Czech Republic and Brno University of Technology, Faculty of Civil Engineering, Institute of Structural Mechanics, Brno, Czech Republic*
*seitl@ipm.cz, http://orcid.org/0000-0002-4953-4324*

**ABSTRACT.** Presented study is focused on the analysis of the dependence of the specific fracture energy value on the assumed work of fracture in three-point bending tests. Specimens of different sizes and relative notch lengths are assumed in this study, in order to take into account the size effect. The three-point bending test of cracked specimens is simulated numerically by means of commercial software based on the finite element method with implemented cohesive crack model. Three levels of the specific fracture energy are considered.

**KEYWORDS.** Specific fracture energy; Finite element method; Work of fracture; Three-point bending test; Loading curve.

**Citation:** Klon, J., Sobek, J., Malíková, L., Seitl, S., Impact of specific fracture energy investigated in front of the crack tip of three-point bending specimen, Frattura ed Integrità Strutturale, 41 (2017) 183-190.

**Received:** 28.02.2017
**Accepted:** 15.04.2017
**Published:** 01.07.2017



## INTRODUCTION

Evaluation of the fracture parameters from experimental data measurement is usually accompanied by numerical calculations. This is unavoidable for example for the quasi-brittle materials, because the process of the failure is not uniform and depends on the test specimen size, shape and also on the boundary conditions during the test itself [1–10]. In the case of these materials, the so-called fracture process zone (FPZ) is situated near the crack tip but its size cannot be seen like in the case of the ductile materials (by range of the plastic zone) [11]. Therefore, some efforts have been made in order to identify the FPZ by means of numerical calculations and investigate its impact on the fracture

process. Currently, many numerical tools can predict fracture behaviour – but just in the case that the proper material parameter inputs are available, like the specific fracture energy.

This paper focuses on the investigation of the impact of the specific fracture energy $G_f$ used in the numerical calculation on the work of fracture $W_f$, which can be obtained by means of evaluation of the loading diagram. The idea of this research is based on the general problem of numerical testing when the current material properties obtained from the experimental testing shall be used. Determination of properties like fracture energy relates to the evaluation of experimental *l-d* (load-deflection) curves. Then the area under the curve is considered. But, if this value of fracture energy shall be used in numerical calculation, there is a restriction – it is not possible to use it due to the fact that it varies by order of the magnitude in dependence on many various factors, such as specimen size, boundary conditions and others. Value of the fracture energy $G_F$ is obtained from the area under the loading curve as work of fracture $W_f$ divided by the area of the cracked ligament $A_f$ (without the initial crack area), so $G_F = W_f / (a-a_0)/B$. Fracture failure of quasi-brittle materials occurs in FPZ by micro cracking (but micro cracks are closed after final failure of the test specimen), so there is a hypothetical problem of accurate evaluation of cracked ligament area $A_f$. It is believed that this is the main reason why the value of $G_F$ (identified from various experimental testing) strongly differs. Therefore, an iteration procedure how to optimize the inputs needs to be performed to include the real *l–d* diagram in numerical calculations. This study shows the impact of the specific fracture energy inputted into numerical software (considering the fracture failure) on the value of the fracture energy obtained from the area under the load–deflection curve (obtained from the numerical calculation). ATENA [12,13] nonlinear software is used for this purpose, so the results are valid mainly for it. For the verification of the impact of the specific fracture energy, the series of experimental test specimens subjected to three-point bending was chosen with the geometry displayed in Fig. 1. Four different sizes of test specimens were created by Ch. Hoover ([14], see the next section) for the purpose of validation of the size effect [1], [7]. In the paper, two approaches are compared. First uses the area under the load–deflection curve to obtain $G_{F(num)}$. This *l–d* curve is obtained from the numerical model (created in ATENA sw.) with the inputted value of the specific fracture energy $G_f$ (three various levels). The latter approach is the theoretical one – the value of the fracture energy is obtained from the basic formula $G_{F(theor)} = G_f (a-a_0) B$.

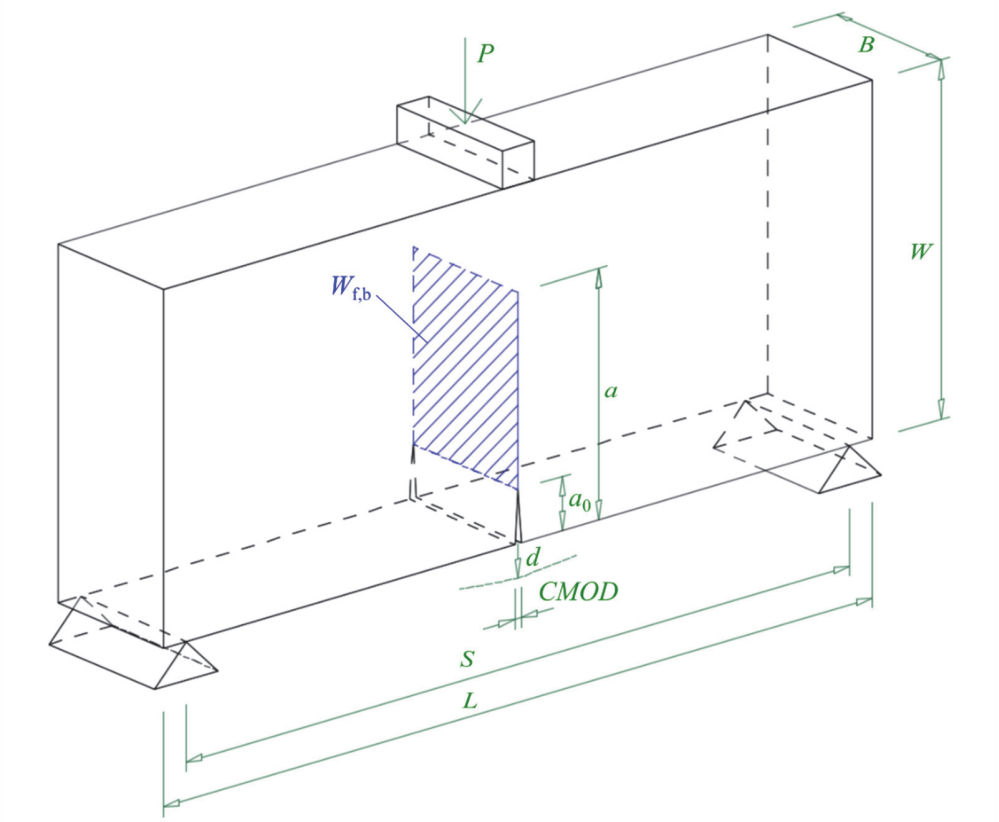


Figure 1: Schema of the three-point bending test configuration. Green color indicates dimensions of the test specimen (see Tab. 1) and CMOD – crack mouth open displacement; blue color represents area of the ligament, where the crack propagation is indicated.

| Specimen | | Width $W$ [mm] | Initial crack length $a_0$ [mm] | Rel. crack length $\alpha_0 = a_0/W$ | Length $L$ [mm] | Span $S$ [mm] | Breadth $B$ [mm] | Crack length $a - a_0$ [mm] |
|---|---|---|---|---|---|---|---|---|
| | | | 3 | 0.075 | | | | 25 |
| D 040 | D | 40 | 6 | 0.15 | 96 | 87.04 | 40 | 22 |
| | | | 12 | 0.3 | | | | 16 |
| | | | 6.98 | 0.075 | | | | 58.12 |
| D 093 | C | 93 | 13.95 | 0.15 | 223.2 | 209 | 40 | 51.15 |
| | | | 27.9 | 0.3 | | | | 37.20 |
| | | | 16.13 | 0.075 | | | | 134.37 |
| D 215 | B | 215 | 32.25 | 0.15 | 516 | 467.84 | 40 | 118.25 |
| | | | 64.5 | 0.3 | | | | 86 |
| | | | 37.5 | 0.075 | | | | 312.5 |
| D 500 | A | 500 | 75 | 0.15 | 1200 | 1088 | 40 | 275 |
| | | | 150 | 0.3 | | | | 200 |

Table 1: Nominal specimen dimensions tested in [14, 15]; the estimated crack length (width of ligament) are shown in the right column.

## THEORY BACKGROUND

### *ATENA software*

ATENA 2D finite-element method (FEM) computational software [12,13] was used – the tool for modelling of structures damaged by cracks. Not only the crack formation, but also their further propagation in dependence on the loading process (increase of force/deflection) can be investigated. Nonlinear material models – such as fracture, plasticity and damage – are included in this sw. to simulate 'real' behavior of the studied material. Fracture-plastic material model for simulation of quasi-brittle materials (concrete) – which is used for all configurations – combines the constitutive models for tensile (fracture) and compressive (plastic) behavior. The model of fracture is based on orthotropic formulation of smeared cracks with crack band model implementation (cohesive crack model).

### *Evaluation of loading diagrams*

The total amount of the dissipated energy (work of fracture $W_{f,b}$) can be determined from the recorded $P-d$ curves, or from the recalculated $R-a$ curves (both methods give the same results). Heron's formula enables to evaluate the dissipated energy from recorded $P-d$ curves. This formula works with the area of a triangle defined by its corners in Cartesian coordinate system. In this case, triangles are formed by origin of coordinate system and two consecutive points of loading diagrams [15]. The last point corresponds to the relative crack length 0.7 ($\alpha = 0.7$), see the schema in Fig. 2. Then, the areas of all triangles are summed.

Recorded $P-d$ curve can be also transformed into the $R-a$ curve (or possibly $R-\alpha$, where $\alpha = a/W$ is the relative crack length). In this transformation, the equivalent elastic crack model [16] is employed for estimation of the current (effective) crack length $a$ at an arbitrary stage of the fracture process (this is the way how to identify the point, when the crack reached the relative length 0.7, as mentioned above). The crack length $a$ is determined from the difference between the initial compliance of the specimen with the crack of length $a_0$ and the specimen compliance at the current point of the $P-d$ diagram. Then, the value of fracture resistance $R$ is calculated from the current load and effective crack length (for each point of the loading diagram), most conveniently as

$$R = \frac{K_{Ic}^2}{E} = \frac{1}{E}\left(\sigma(P)\sqrt{a}\,Y(\alpha)\right)^2 \quad [\mathrm{J/m^2}], \tag{1}$$

where $\sigma(P)$ is the nominal stress in the line of the crack in the specimen due to the load $P$ and $Y(\alpha)$ is the corresponding geometry function. Thus, the corresponding point of $R-a$ curve is calculated for each point of $P-d$ curve. The value of $W_{f,b}$ calculated from area under $P-d$ curve is equal to the area under the $R-a$ curve. Transformation of the $P-d$ diagram into the $R-\alpha$ curve with indication of meanings of $W_{f,b}$, is shown in Fig. 2 and Fig. 3.

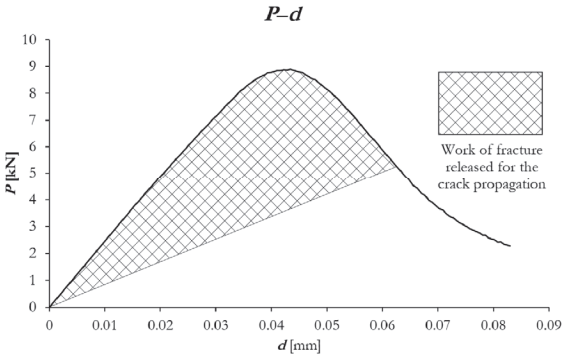


Figure 2: Work of fracture indication at the current stage of fracture process in the loading diagram (peak-deflection curve).

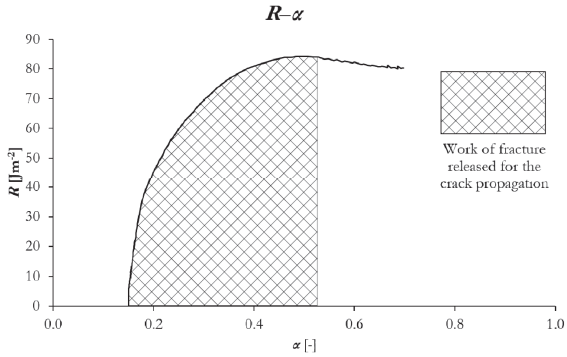


Figure 3: Work of fracture indication at the current stage of fracture process in the *R*-curve.

*Experiment made by Hoover et al.*

In the experimental campaign reported in [14], four beam sizes of widths $W$ = 500, 215, 93 and 40 mm (marked as A to D, see) with three relative notch lengths $\alpha_0$ = 0.075, 0.15, and 0.3 were subjected to three-point bending tests. Ratio of the smallest and the largest tested specimen is remarkable, namely 1:12.5. Several samples were tested for each $W$ and $\alpha_0$, for details see [14]. Nominal dimensions of the test specimen are shown in Tab. 1.

## NUMERICAL MODELS

Numerical models (see Fig. 4 to 7) were created with respect to the geometry given in Fig. 1 and Tab. 1 and the plane stress conditions were met. Connection of steel loading platens with concrete in the part around the groove is solved by using contact elements due to more realistic behavior of platens during the load process by increment of deformation (as a function of load step). Monitoring points were used to observe values of horizontal and vertical displacements and applied forces (reactions).

Material model (in ATENA sw. referred to as 3D Non Linear cementitious 2) was used for the simulation of the quasi-brittle specimen with following parameters: Young's modulus $E$ = 34 GPa, Poisson's ratio $\nu$ = 0.172, tensile strength $f_t$ = 5.40 MPa, compressive strength $f_c$ = 49.00 MPa, three levels of specific fracture energy $G_f$ = 7; 70; 700 N/m, Hordijk's exponential softening. The finite element mesh was generated with regard to the area of the expected extent of FPZ (Fig. 4) with finite element size of 1 mm. Steel loading platens were modelled by 2D elastic isotropic material model with $E$ = 210 GPa and $\nu$ = 0.3.

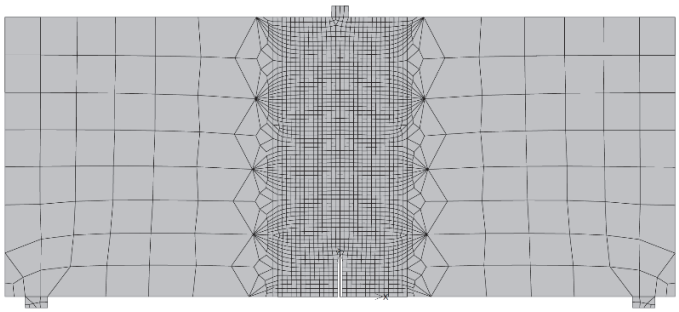

Figure 4: Numerical model of the test specimen D 500 with the initial relative crack length $\alpha_0$ = 0.15; detail of the FE mesh in ATENA 2D software.

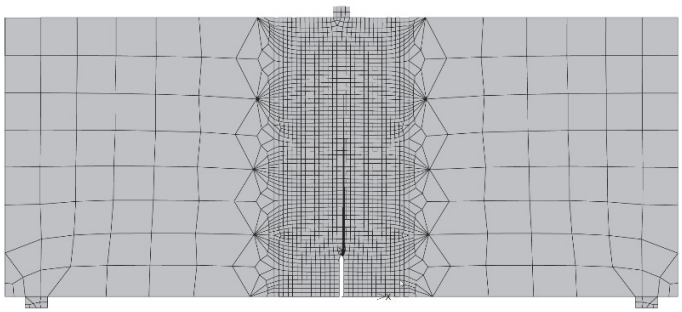

Figure 5: Numerical model of the test specimen D 500 with the initial relative crack length $\alpha_0$ = 0.15; fracture failure at stage $\alpha$ = 0.7 considering the specific fracture energy $G_f$ = 7 N/m.

It is obvious that the response of the test specimen on the loading progress strongly differs in the way of used level of the specific fracture energy $G_f$ (see Fig. 8). For the highest value of $G_f$ = 700 N/m the peak value of the loading force is two times higher than in the case of $G_f$ = 70 N/m (this can be also applied for comparison of the lowest and the middle value of $G_f$). Each value of used $G_f$ has also significant impact on the way of fracture failure (Fig. 9). Brittle fracture corresponds

to the lowest value of specific fracture energy used, middle value represents the quasi-brittle behavior and the highest value of $G_f$ indicates ductile behavior.

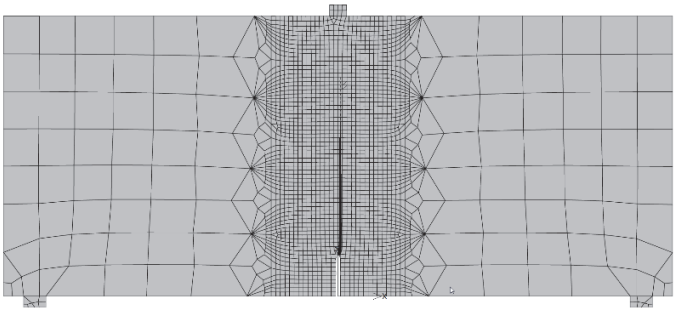

Figure 6: Numerical model of the test specimen D 500 with the initial relative crack length $\alpha_0 = 0.15$; fracture failure at stage $\alpha = 0.7$ considering the specific fracture energy $G_f = 70$ N/m.

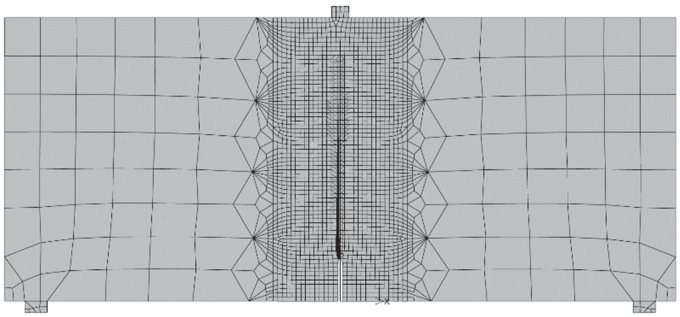

Figure 7: Numerical model of the test specimen D 500 with the initial relative crack length $\alpha_0 = 0.15$; fracture failure at stage $\alpha = 0.7$ considering the specific fracture energy $G_f = 700$ N/m.

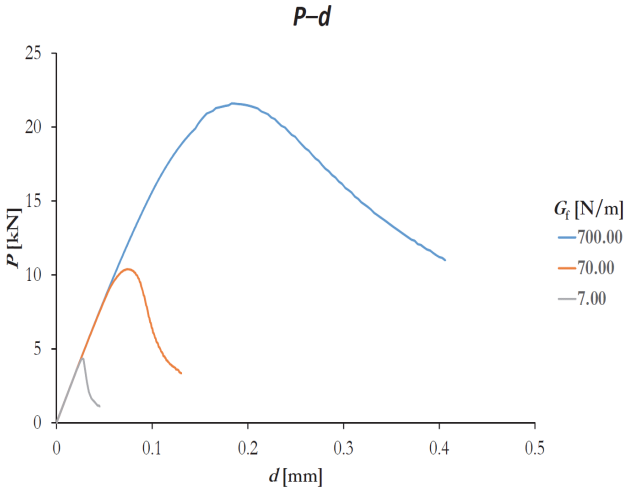


Figure 8: Scale illustration of the progress of the loading diagram (peak-deflection curve) for all variants of the specific fracture energy used.

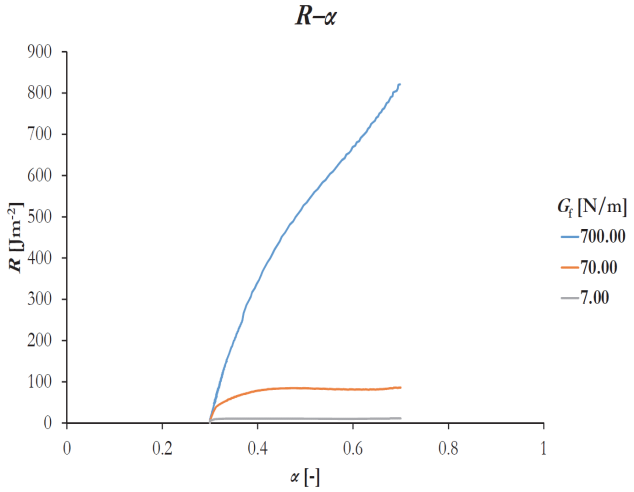


Figure 9: Scale illustration of the progress of the *R*-curve for all variants of the specific fracture energy used.

## DISCUSSION OF RESULTS

As can be seen from Fig. 10, 11 and 12 the quantity of the dissipated energy is different for various specimen sizes and for various initial notch lengths. As expected, the amount of the dissipated energy is also changing according to the selected level of the specific fracture energy. The amount of the dissipated energy is dependent on the specimen size due to increasing ligament area. When the specimen size is larger, the amount of the dissipated energy increases. As was already mentioned – the amount of the energy dissipated during crack growth from the initial notch to the relative length $a/W = 0.7$ was considered. Ligament area grows approximately 2.3 times for two consecutive specimen sizes. The dissipated energy obtained by means of theoretical calculations $G_{F(theor)}$ corresponds to this expectation. This ratio was achieved for all three selected values of the specific fracture energy via the theoretical calculation: for the dissipated energy determined from the FEM analysis, this proportion was reached (with a deviance of 20 %) for the middle value of the specific fracture energy. The middle level of the specific fracture energy was chosen according to available loading diagrams for the actual cement composite used for preparation of the test specimens published in [12]. Its real value of specific fracture energy was $G_f = 70$ N/m. If the higher order value of the specific fracture energy $G_f = 700$ N/m is used the current ratio does not apply. It can be seen in Fig. 12. At this level, the amount of the energy

dissipated in small specimens is much more less than it should correspond to the current area of the specimen's ligament. For example, the specimen D 040 with the initial notch $\alpha_0 = 0.075$ has the amount of the dissipated energy smaller by 75 % than the value obtained by theoretical calculations. With the increasing size of the specimen the deviation is reducing as much, that for the biggest specimen (D 500) the ratio of the dissipated energy is almost 2.9 times bigger than in the case of the smaller one (D 215). Comparison of the values of the dissipated energy obtained by FEM analysis and theoretical calculation for specimen D 500 with the initial notch of the length $\alpha_0 = 0.075$ shows the deviation under 20 %. This phenomenon is repeated for all initial notch length variants. The deviations varied from 80 % (small specimens of size D 040) to 30 % (the biggest specimens of size D 500). The opposite trend was observed for the specimens with the low order of value of the specific fracture energy $G_f = 70$ N/m. For the smallest specimens, the deviation from the theoretical calculation was lower than for the biggest specimens. While the dissipated energy determined from FEM analysis for the small specimen D 040 reaches the maximum deviation of 13 %, the biggest specimen D 500 exceeds 120 %, see Fig. 12.
Described behavior is certainly related to the way of failure which differs for the selected values of the specific fracture energy. It is clear from Fig. 8, that not only the area under the loading curve but also the maximum reached loading force changes. The peak force is approximately two times bigger comparing two subsequent values of the specific fracture energy $G_f$. Similarly, the specimen response is also changing with the level of the specific fracture energy used: the response of the specimen with the middle level of the specific fracture energy corresponds to the quasi-brittle fracture. Fracture progress in the specimen with the lower level of the specific fracture energy corresponds to brittle fracture, where the FPZ does not develop. Significant ductile behavior is typical for the highest level of the specific fracture energy used. This tendency can be seen in Fig. 5 to 7 where the finite element mesh is shown and the way of fracture failure for each level of the specific fracture energy. It is obvious that the wider band of elements is damaged by cracks for the higher level of the specific fracture energy than in the case of the lower one (FPZ is not developed). This behavior is probably caused by the use of the crack band model, that is implemented in ATENA 2D software tool.
It is clear from the displayed results that it is necessary to pay attention to the use of the proper level of the specific fracture energy when ATENA tool shall be used for modelling of structures and following evaluation of results. It was found out that the selected value of the specific fracture energy reflects not only the total amount of the dissipated energy during fracture, but also maximum loading force achievement and the way of structural response.

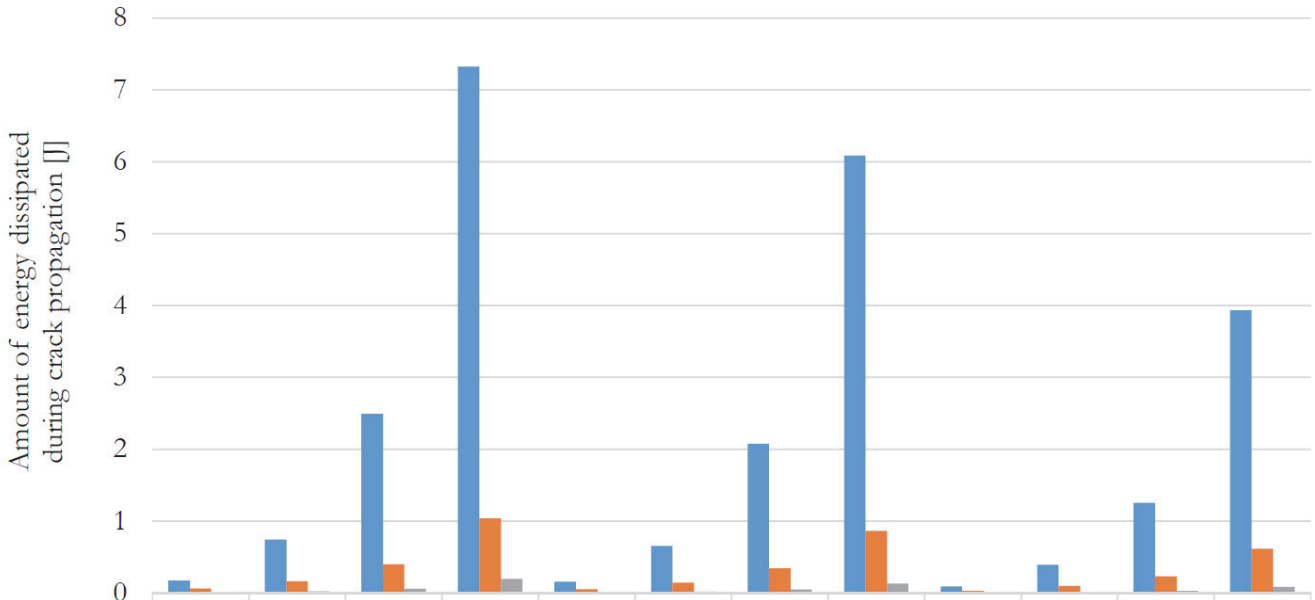


| | α | Spec. size | $G_f$ [N/m] |
|---|---|---|---|
| 0.075 | 0.075 | D 040 | 700.00 |
| 0.075 | 0.075 | D 093 | 700.00 |
| 0.075 | 0.075 | D 215 | 700.00 |
| 0.075 | 0.075 | D 500 | 700.00 |
| 0.15 | 0.15 | D 040 | 700.00 |
| 0.15 | 0.15 | D 093 | 700.00 |
| 0.15 | 0.15 | D 215 | 700.00 |
| 0.15 | 0.15 | D 500 | 700.00 |
| 0.30 | 0.30 | D 040 | 700.00 |
| 0.30 | 0.30 | D 093 | 700.00 |
| 0.30 | 0.30 | D 215 | 700.00 |
| 0.30 | 0.30 | D 500 | 700.00 |
| 0.1712 | 0.7414 | 2.4879 | 7.3228 |
| 0.1556 | 0.6547 | 2.0727 | 6.0850 |
| 0.0869 | 0.3913 | 1.2523 | 3.9312 |
| 0.0585 | 0.1639 | 0.3983 | 1.0375 |
| 0.0522 | 0.1416 | 0.3406 | 0.8621 |
| 0.0294 | 0.0966 | 0.2318 | 0.6119 |
| 0.0074 | 0.0193 | 0.0564 | 0.1944 |
| 0.0069 | 0.0175 | 0.0471 | 0.1273 |
| 0.0047 | 0.0146 | 0.0291 | 0.0815 |

Figure 10: Value of the fracture energy $G_{F(num)}$ dissipated during the crack propagation for all variants of numerical models – obtained from the area under the *l-d* curve (*R–a* diagram respective) simulated in ATENA.

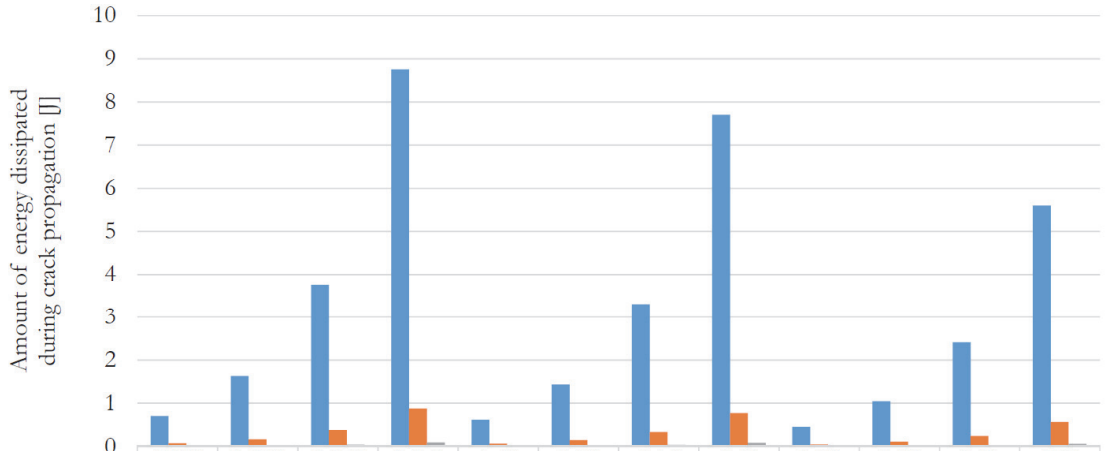


| | α | 0.075 | 0.075 | 0.075 | 0.075 | 0.15 | 0.15 | 0.15 | 0.15 | 0.30 | 0.30 | 0.30 | 0.30 |
|---|---|---|---|---|---|---|---|---|---|---|---|---|---|
| | Spec. size | D 040 | D 093 | D 215 | D 500 | D 040 | D 093 | D 215 | D 500 | D 040 | D 093 | D 215 | D 500 |
| $G_f$ [N/m] | 700.00 | 0.7000 | 1.6275 | 3.7625 | 8.7500 | 0.6160 | 1.4322 | 3.3110 | 7.7000 | 0.4480 | 1.0416 | 2.4080 | 5.6000 |
| | 70.00 | 0.0700 | 0.1628 | 0.3763 | 0.8750 | 0.0616 | 0.1432 | 0.3311 | 0.7700 | 0.0448 | 0.1042 | 0.2408 | 0.5600 |
| | 7.00 | 0.0070 | 0.0163 | 0.0376 | 0.0875 | 0.0062 | 0.0143 | 0.0331 | 0.0770 | 0.0045 | 0.0104 | 0.0241 | 0.0560 |

Figure 11: Value of the fracture energy $G_{F(theor)}$ dissipated during the crack propagation for all variants of numerical models – obtained from theoretical calculation.

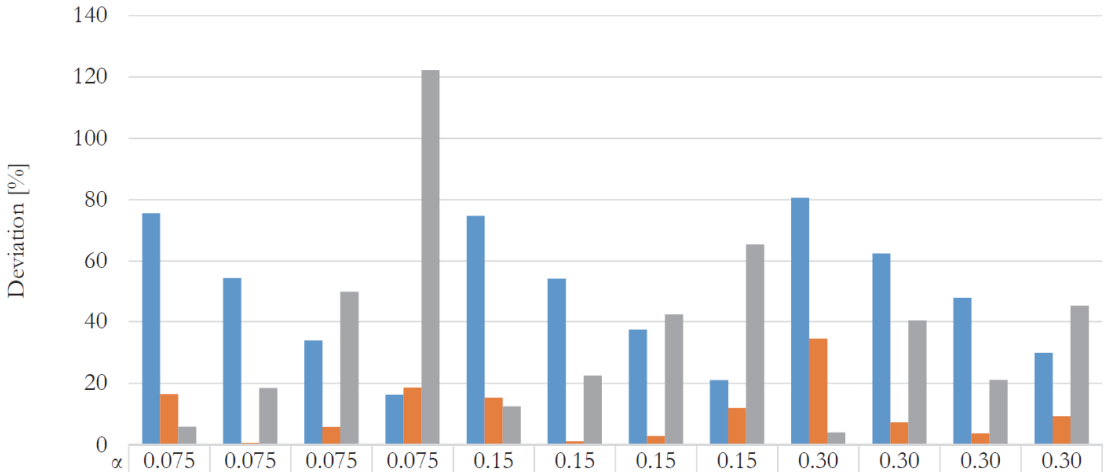


| | α | 0.075 | 0.075 | 0.075 | 0.075 | 0.15 | 0.15 | 0.15 | 0.15 | 0.30 | 0.30 | 0.30 | 0.30 |
|---|---|---|---|---|---|---|---|---|---|---|---|---|---|
| | Spec. size | D 040 | D 093 | D 215 | D 500 | D 040 | D 093 | D 215 | D 500 | D 040 | D 093 | D 215 | D 500 |
| $G_f$ [N/m] | 700.00 | 75.54 | 54.45 | 33.88 | 16.31 | 74.73 | 54.28 | 37.40 | 20.97 | 80.60 | 62.43 | 47.99 | 29.80 |
| | 70.00 | 16.44 | 0.68 | 5.85 | 18.57 | 15.31 | 1.14 | 2.88 | 11.96 | 34.43 | 7.30 | 3.75 | 9.27 |
| | 7.00 | 5.89 | 18.42 | 50.00 | 122.21 | 12.51 | 22.51 | 42.31 | 65.37 | 4.06 | 40.30 | 21.02 | 45.46 |

Figure 12: Deviation between the values of $G_{F(num)}$ and $G_{F(theor)}$ dissipated during the crack propagation for all variants of numerical models.

## CONCLUSIONS

The paper presents a study on the impact of the value of the specific fracture energy inputted into FE software (considering the fracture failure) on the amount of the energy dissipated during quasi-brittle fracture. Three-point bending tests of specimens with different size and initial notch length was subject of this study. The amount of the dissipated energy was examined by using two methods. The first method consists in the numerical FEM analysis; the amount of the energy was obtained from the area under the loading curve obtained from numerical simulations. The latter

one consists in multiplication of the value of the specific fracture energy (inputted into ATENA software) with the area of ligament. Three values of the specific fracture energy were considered: $G_f$ = 7; 70; 700 N/m. Specimens of four sizes with the same geometry proportions were assumed to reflect the impact of the size effect. The results obtained show a strong dependence of the amount of the dissipated energy during fracture on the value of the specific fracture energy considered for calculations. Similarly, a significant dependence of the maximum achieved loading force on the value of the specific fracture energy was observed. Therefore, it is crucial to set the proper value of the specific fracture energy when more complex fracture analyses need to be performed in order to avoid misleading results.
Note that the authors intend to extend the study on the impact of the specific fracture energy value on the amount of the energy dissipated to the wedge splitting test geometry.

## ACKNOWLEDGEMENT

This paper has been worked out under the project of the Czech Science Foundation (project No. 15-07210S).

## REFERENCES

[1] Bažant, Z.P., Kazemi, M.T., Size dependence of concrete fracture energy determined by RILEM work-of-fracture method, Int. J. Fract., 51(2) (1991) 121–138.
[2] Elices, M., Guinea, G. V., Planas, J., Measurement of the fracture energy using three-point bend tests: part 3–Influence of cutting the P–δ tail, Mater. Struct., 25(6) (1992) 327–334.
[3] Hu, X.-Z., Wittmann, F.H., Size effect on toughness induced by crack close to free surface. Engng. Fract. Mech., 65 (2000) 209–221.
[4] Trunk, B., Wittmann, F.H., Influence of size on fracture energy of concrete, Mater. Struct, 36 (2001) 260–265.
[5] Karihaloo, B.L., Abdalla, H.M., Imjai, T., A simple method for determining the true fracture energy of concrete. Mag. Concr. Res., 55 (2003) 471–481.
[6] Duan, K., Hu, X.-Z., Wittmann, F.H., Boundary effect on concrete fracture and non-constant fracture energy distribution, Engng. Fract. Mech., 70 (2003) 2257–2268.
[7] Bažant, Z.P., Yu, Q., Size effect in fracture of concrete specimens and structures: new problems and progress, in Li V.C. et al. (eds.), Proc. of the 5th international conference on fracture mechanics of concrete and concrete structures, Vail Colorado, USA, (2004) 153–162.
[8] Hu, X.-Z., Duan, K., Size effect: Influence of proximity of fracture process zone to specimen boundary, Engng. Fract. Mech., 74 (2007) 1093–1100.
[9] Yu, Q., Le, J., Hoover, C., Bažant, Z., Problems with Hu-Duan Boundary Effect Model and its comparison to Size-Shape Effect Law for quasi-brittle fracture, J. Eng. Mech., 89 (2010) 40–50. DOI: 10.1061/(ASCE)EM.1943-7889.
[10] Cifuentes, H., Alcalde, M., Medina, F., Measuring the size-independent fracture energy of concrete, Strain, 49(1) (2013) 54–59.
[11] Suresh, S., Fatigue of Materials, Cambridge University Press, (1998) 679.
[12] Červenka, V., Jendele, L., Červenka, J., ATENA Program Documentation, Cervenka Consulting, Prague (2010).
[13] Červenka, V., Červenka, J., Pukl, R., ATENA / A tool for engineering analysis of fracture in concrete, Sadhana-Adacemy Proceedings in Engineering Sciences, 27 (2002) 485–492.
[14] Hoover, Ch.G., Bažant, Z.P., Vorel, J., Wendner, R., Hubler, M.H., Comprehensive concrete fracture tests: Description and results, Engng. Fract. Mech., 114 (2013) 92–103.
[15] Klon, J., Veselý, V., Modelling of size and shape of damage zone in quasi-brittle notched specimens – analytical approach based on fracture-mechanical evaluation of loading curves, Frattura ed Integrità Strutturale, 39 (2017) 17–28.
[16] Karihaloo, B.L., Fracture mechanics and structural concrete, Longman Sci. & Techn., New York (1995).